# Ab initio density-functional theory study of NHx dehydrogenation and reverse reactions on the Rh(1111) surface

# *Ab initio* density-functional theory study of $NH_x$ dehydrogenation and reverse reactions on the Rh(111) surface

C. Popa,* W. K. Offermans, R. A. van Santen, and A. P. J. Jansen
*Molecular Materials and Nanosystems; Schuit Institute of Catalysis, ST/SKA, Eindhoven University of Technology, P.O. Box 513, NL-5600 MB Eindhoven, The Netherlands*

(Received 26 June 2006; revised manuscript received 28 August 2006; published 24 October 2006)

The adsorption and dissociation of $NH_x$ fragments on the Rh(111) crystal surface have been studied using first-principles density-functional calculations. The stability and configurations of $NH_x$ species have been investigated and characterized using frequency analysis. The highest adsorption energies have been calculated for NH and N. Several paths of $NH_x$ ($x=1-3$) dehydrogenation and hydrogenation have been taken into account. The transition states have been determined and in detail analyzed. The activation barriers and thermodynamic and kinetic data have been calculated for all the elementary steps. The calculations have shown that the elementary reactions have significant barriers, between 0.7 and 1.1 eV. The transition states are regarded neither early nor late with respect to the distance in hyperspace between initial and final states. The $NH_3$ dehydrogenation has been determined as the rate limiting step. For this elementary process there has been estimated a large contribution of the zero point energy to the activation barrier and a significant entropy activation.

DOI: 10.1103/PhysRevB.74.155428 PACS number(s): 31.50.Bc, 31.15.Ew, 82.20.Db, 82.65.+r

## I. INTRODUCTION

Understanding the atomistic processes which occur in heterogeneous catalysis is a big challenge. Many interesting phenomena are regarded as a sequence of elementary steps such as adsorption, diffusion, and dissociation. These phenomena on transition metals are an important area of surface science and heterogeneous catalysis. The interaction of adsorbates with a particular metallic surface can lead to important consequences for the surface catalyzed reactions. In particular, ammonia dehydrogenation presents an important technological, economic, and environmental problem. It can be used for converting to $N_2$, to reduce the $NO_x$ emissions by selective catalytic reduction (SCR), and also as hydrogen source and storage in fuel cells.[1–3] These processes were experimentally and theoretically studied at different pressures and temperatures, using various catalytic active surfaces. The main interest is to determine the stability of the species and to evaluate the kinetics and thermodynamics of the reaction mechanisms.

Experimentally the ammonia synthesis mechanism on the Rh(111) surface was investigated using temperature programmed desorption (TPD), temperature programmed reaction spectroscopy (TPRS), and static secondary ion mass spectrometry (SSIMS) by Hardeveld *et al.*[2] They found that the $NH_2$ hydrogenation has the highest activation barrier and that the rate of $NH_3$ desorption depends on the coverage. Ganley *et al.*[4] examined experimentally ammonia decomposition on several transition metals, concluding that rhodium is one of the best catalysts. Leewis *et al.*[5] presented direct evidence about the presence of $NO_x$ intermediates during ammonia formation on the Rh surface. They applied attenuated total reflection Fourier transform infrared spectroscopy (ATR-FTIR) to study $NH_3$ decomposition on Rh nanoparticles and detected bend and stretch vibrations and assigned to the $NO_x$ intermediates between 20 and 100 °C.

Also theoretical studies were dedicated to $NH_3$ on several clean *d*-band metallic surfaces, as Rh,[6,7] Ni, Pd,[3] Ru,[8,9] Pt,[10,11] and Au.[12] On Rh Frechard *et al.*[6] studied the ammonia adsorption on different surfaces. They concluded that for the $NH_3$ adsorbed molecule the top site is the most stable position. A first estimate of the energetics for the ammonia synthesis was presented by Liu *et al.* and Crawford *et al.*[7,13] They searched the transition states by constraining the H-$NH_x$ distance as the reaction path. In fact there are many questions to be further addressed concerning the stability of the $NH_x$ species and transition states on the potential energy surface and kinetic and thermodynamic characteristics of catalytic phenomena derived from *ab initio* data.

In this paper we present a detailed *ab initio* density-functional investigation of the reaction profile for the ammonia dehydrogenation on the Rh(111) surface. First we discuss in detail the stability of the H-$NH_x$ fragments and their vibrations. Then we focus on the determination of different possible transition states for the dissociation reactions. The $NH_x$ species are characterized using vibrational analysis. Finally, the kinetic and thermodynamic parameters of the dehydrogenation and hydrogenation reactions are determined via partition functions and discussed.

Our paper is organized as follows. In Sec. II we briefly review the computational aspects. We introduce the method for calculating kinetic parameters using statistical thermodynamics and the method of finding transition states. Section III contains results and discussions. Herein Sec. III A we discuss the adsorption and coadsorption of the $NH_x$ fragments on the Rh(111) surface. In Sec. III B we discuss the frequency analysis and comparison with the available experimental data. Section III C presents the results for determination of the transition states, and the general scenario for $NH_3$ dehydrogenation. Section III D discusses the thermodynamic and kinetic parameters. The transition-state activation energies are given for the dehydrogenation and the reverse reactions of $NH_x$ hydrogenation. Section IV presents our conclusions.

 

## II. COMPUTATIONAL DETAILS

The electronic structure calculations were performed using density-functional theory (DFT) with the Vienna Ab Initio Simulation Package (VASP)[14,15] code, with a plane wave basis set, ultrasoft Vanderbilt pseudopotentials,[16] and the generalized gradient approximation (GGA)[17] for the exchange and the correlation energy proposed by Perdew and Wang.[18] Tests showed that the spin contribution to the total energy of the adsorbated systems is negligible and hence a spin-restricted approach was used[19–21] except for the atoms and molecules in gas phase. With the considered pseudopotentials, a cutoff energy of 400 eV for the plane wave basis ensures a good accuracy. For the Brillouin zone integration a Monckhorst Pack $5\times5\times1$ mesh was used for all structures.

The Rh(111) surface was modeled with the slab supercell approach. A $p(2\times2)$ unit cell was used which consisted of five layers of metal, which were allowed to fully relax, and an equivalent vacuum space (11.1 Å) in the $z$ direction between successive slabs. The optimized bulk nearest-neighbor separation of 2.72 Å is in good agreement with the experimental value of 2.69 Å.[22] The molecules were adsorbed on both sides of the metallic slab with a $S_2$ symmetry center to avoid long-range dipole-dipole interactions between translational equivalent unit cells. Tests performed with different values of cutoff energy and different number of $k$-points showed that the convergence of the total energy is within $5\times10^{-2}$ eV. The conjugate-gradient algorithm was used to relax the ions into their equilibrium locations. Equilibrium is reached if the Hellmann-Feynman forces on the atoms are less than 0.02 eV Å$^{-1}$ in each of the Cartesian directions. For the structures which we have performed vibrational analysis the forces were smaller than $10^{-3}$ eV Å$^{-1}$ and the energy convergence smaller than $10^{-6}$ eV. As a comparison with the $p(2\times2)$ unit cell we used a $p(3\times3)$ unit cell in one instance (see Sec. III A, but all other computational parameters were the same).

The adsorption energy for all the high symmetry adsorption sites of the $NH_x$ fragments was calculated according to the equation

$$E_{\mathrm{ads}}=[E_{\mathrm{NH}_x/\mathrm{Rh}}-E_{\mathrm{Rh}}-nE_{\mathrm{NH}_x(\mathrm{gas})}]/n, \tag{1}$$

where $E_{\mathrm{NH}_x/\mathrm{Rh}}$ is the total energy of the $NH_x$ system adsorbed on the Rh surface, $E_{\mathrm{Rh}}$ is the energy of the metallic slab, $E_{\mathrm{NH}_x(\mathrm{gas})}$ is the energy of the $NH_x$ fragment in gas phase, and $n$ is the number of the $NH_x$ (co)adsorbates on the slab.

Vibrational frequencies were computed for the initial and final states as well for the transition states in the harmonic approximation as the method is incorporated in VASP. We applied a finite displacement in all directions, for the first layer Rh atoms and for the adsorbates. The second derivatives of the potential energy surface were used to calculate the dynamical matrix. By diagonalization of this matrix the frequencies and the surface phonons and the associated normal modes are obtained. A reasonable value of the finite displacement is ±0.02 Å, as a compromise between the accuracy of the force calculation and harmonic approximation. However, in the case of almost flat potential energy surfaces with respect to the degrees of freedom for adsorbates 0.01 Å seems to be better to avoid anharmonicities. Tests showed that the phonons of the inner metallic layers almost do not couple with the frequencies of the adsorbated fragments. This fact makes it possible to freeze the degrees of freedom of the inner metallic atoms in the frequency calculations.

Using DFT the experimental vibrational frequencies are usually reproduced within a few percent accuracy.[23,24] The errors become larger the more complicated the vibrations are and the stronger anharmonic and long range electric forces are. It has been shown for different types of systems (small molecules adsorbed on metallic surfaces, DNA, RNA, diamond, carbon nanotubes, zeolites, etc.) that the calculated frequency optical bands using the VASP program were in reasonable agreement with the experiments.[23,25–28] Despite the systematic error inherent in the GGA exchange-correlation and various numerical approximations, the computed frequencies are accurate to 2 to 3 %.[29]

The nudged elastic band method (NEB) implemented in the VASP program was used to determine the dissociation paths.[30,31] The minimum energy path (MEP) relates the initial ($NH_x$) and the final ($NH_{x-1}+H$) states by a set of intermediate states connected by the elastic band and distributed along the reaction coordinate. Each state is fully relaxed in the hyperspace perpendicular to the energy path. For difficult cases we used the climbing image NEB or the variable NEB methods.[32–34] Depending on the energy profile, we used 8–16 images for a NEB calculation. After dissociation, $NH_{x-1}$ and H are coadsorbed on the surface. The adsorption energies were calculated according to Eq. (1). The barrier energy of the dissociation reaction is given by the difference between the energies of the transition state (TS) and of the $NH_x$ fragment (reactant, R) which will dissociate. The NEB calculation gives a configuration which is a good candidate for the transition state structure. After minimizing the residual forces, a vibrational analysis is used to check if indeed a transition state was found. If a molecule is in a real minimum of the potential energy surface, all frequency values are positive; and a true transition state is a saddle point on the PES and must have one, and only one, imaginary frequency corresponding to the reaction path degree of freedom.

For a single step reaction the rate constant at temperature $T$ can be written in an Arrhenius type expression:

$$k=\nu^{*}e^{-E_{act}/k_{\mathrm{B}}T}, \tag{2}$$

where $\nu^{*}$ is the preexponential factor, $E_{act}$ is the activation energy, and $k_{\mathrm{B}}$ is the Boltzmann constant.

If we assume the validity of the harmonic transition state theory and use the partition functions for reactants and transition states ($Q_{\mathrm{R}},Q_{\mathrm{TS}}$), it is possible to calculate also the activation energy and the preexponential factor of a reaction. In the harmonic transition state theory the rate constant for a reaction can be calculated as

$$k=\frac{k_{\mathrm{B}}T}{h}\frac{Q_{\mathrm{TS}}}{Q_{\mathrm{R}}}e^{-(E_{\mathrm{TS}}-E_{\mathrm{R}})/k_{\mathrm{B}}T}, \tag{3}$$

where $E_{\mathrm{TS}}-E_{\mathrm{R}}=E_{\mathrm{bar}}$ is the difference between the energies of the transition state and of the reactants, the activation barrier.

TABLE I. Adsorption energies on the $p(2\times2)$-Rh(111) surface (eV molecule$^{-1}$). The ZPE corrected adsorption energies are given in parenthesis. The values are given with respect to the $NH_x$ fragments and atoms in the gas phase. The gas phase energies were calculated in large unit cells, taking into account also the spin contribution (in eV molecule$^{-1}$: $NH_3$: −19.58, $NH_2$: −13.56, NH: −8.18, N: −3.44, H: −1.12, $N_2$: −16.52, and $H_2$: −6.80).

| System | Top | Bridge | fcc | hcp |
|---|---|---|---|---|
| $NH_3$ | −0.75 (−0.65) | −0.17 | −0.12[a] | −0.12[a] |
| $NH_2$ | −2.12[a] | −2.75 (−2.56) | −2.42 | −2.43[a] |
| NH | −2.46 | −3.72[a] | −4.36 (−4.17) | −4.35 (−4.17) |
| N | −3.03[a] | −4.45[a] | −4.95 (−4.86) | −5.07 (−4.98) |
| H | −2.42 (−2.25) | −2.73 (−2.58) | −2.84 (−2.68) | −2.81 (−2.65) |

[a]Restricted geometry optimization.

The partition functions of the adsorbed species can be calculated using the normal mode frequencies. The total partition function including the zero point energy (ZPE) correction can be written as

$$Q = \prod_{i=1}^{3N} \frac{e^{-h\nu_i/2k_BT}}{1-e^{-h\nu_i/k_BT}}, \tag{4}$$

where $\nu_i$ are the frequencies of the vibration modes.[35,36] The potential energy surface (PES) can be almost flat for rotations. We encounter this situation for the ammonia molecule adsorbed on top. $NH_3$ can rotate freely around its threefold axis. In this case the partition function for rotation around an axis perpendicular to the surface is given by the expression

$$Q_{2D} = \frac{2\pi}{h}\sqrt{2\pi I k_B T}, \tag{5}$$

where $Q_{2D}$ is the partition function of a two-dimensional (2D) rotator and $I$ is the inertial moment of the rotor. From the expressions derived for the partition functions, we can calculate the entropy

$$S = k_B \ln Q + k_B T\left(\frac{\partial \ln Q}{\partial T}\right)_{N,V} \tag{6}$$

for a system with constant volume ($V$) and number of particles ($N$).

Using Eq. (3) the activation energy which includes also the ZPE is given by the following equation:

$$E_{act,0} = k_B T^2 \frac{\partial \ln k_{diss}}{\partial T} = \Delta H^{\#}_{diss,0} + k_B T, \tag{7}$$

where $\Delta H^{\#}_{diss,0}$ is the activation enthalpy. For high activation barriers $k_BT$ becomes negligible and $E_{act,0} \approx \Delta H^{\#}_{diss,0}$. The expression from harmonic transition state theory for the activation energy will give values very close to the experimental values obtained by fitting the Arrhenius expression [Eq. (2)] to rate constants over a temperature range.

The preexponential factor can be calculated as

$$\nu^* = \frac{e k_B T}{h} e^{\Delta S^{\#}_0/k_B} \tag{8}$$

with $\Delta S^{\#}_0$ being the activation entropy for a reaction.[36]

## III. RESULTS AND DISCUSSIONS

### A. $NH_x$ adsorption on the Rh(111) surface

The adsorption energies for $NH_x$ and H are presented in Table I. Calculations performed for $NH_3$ adsorption show that the top site is preferred, with the N atom pointing toward the surface, in agreement with previous studies of ammonia adsorbed on transition metal surfaces.[3,6,7,9–12,37] The adsorption energy is −0.75 eV molecule$^{-1}$ for 0.25 ML coverage [$p(2\times2)$ unit cell] and −0.87 eV molecule$^{-1}$ for 0.11 ML coverage [$p(3\times3)$ unit cell]. The repulsive interactions are smaller for the $p(3\times3)$ unit cell. The value obtained for the adsorption energy is in very good agreement with the theoretical and experimental values, −0.84 and −0.87 eV molecule$^{-1}$.[4,6] The bridge and the hollow sites lead to weak adsorption states.

The ammonia adsorbed on top in a $p(2\times2)$ unit cell is almost perpendicular to the surface (91°) and the Rh–N bond length is 2.18 Å. The HNH angle is 111° and the RhNH angle is 108°. The NH bond length is 1.12 Å. Because of the flatness of the potential energy surface and no symmetry constraints were imposed during geometry optimization (except $S_2$ for the unit cell), the molecule has a small deviation from perpendicularity on the metallic surface. The potential energy surface is quite flat for the rotation of the ammonia around the three-fold axis. The molecule is behaving almost as a free rotor. However, the vibrational analysis shows that not all orientations are stable. The most stable orientation is almost eclipsed (the N–H bonds are along the Rh–Rh bonds), the RhRhNH dihedral angle being 10°. We obtained the highest energy for the staggered position with the N–H bonds in between two Rh–Rh bonds, with a dihedral angle of 30°. The barrier of rotation is very small; 0.003 eV molecule$^{-1}$. The small deviation from the exactly eclipsed position might be due to the asymmetry in the second layer of metal atoms. The vibrational analysis shows that the spinning mode has a very low frequency, of 53.3 cm$^{-1}$, and for the staggered position we obtained one imaginary frequency (−89 cm$^{-1}$). We conclude that the eclipsed mode is the real minimum on the potential energy surface and the staggered position is the maximum.

The bridge site is the most stable one for the $NH_2$ adsorption on Rh(111). The hollow adsorption sites are about

TABLE II. Coadsorption energies of ($NH_x$+H) fragments on $p(2\times2)$-Rh(111) surface, the sum of separate adsorption energies (eV molecule$^{-1}$) and the distances between the N atom and the coadsorbed H atom. The ZPE corrected coadsorption energies are given in parenthesis.

| System | $d_{N\text{-}H}$ (Å) | $E_{coads}(NH_x+H)$ | $E_{ads}(NH_x)+E_{ads}(H)$ |
|---|---|---|---|
| $NH_2$ bridge+H fcc | 2.51 | −5.37 | −5.59 |
| | 2.93 | −5.48 | −5.59 |
| $NH_2$ bridge+H hcp | 2.51 | −5.32 | −5.56 |
| | 2.96 | −5.47 (−5.11) | −5.56 |
| NH fcc+H fcc | 3.01 | −6.96 (−6.60) | −7.20 |
| NH fcc+H hcp | 3.37 | −7.02 | −7.17 |
| NH hcp+H fcc | 3.37 | −7.05 (−6.71) | −7.20 |
| NH hcp+H hcp | 3.00 | −6.93 (−6.58) | −7.17 |
| N fcc+H fcc | 2.73 | −7.52 (−7.26) | −7.79 |
| N fcc+H hcp | 2.73 | −7.60 | −7.76 |
| N hcp+H fcc | 3.14 | −7.63 (−7.37) | −7.91 |
| N hcp+H hcp | 2.72 | −7.60 (−7.34) | −7.88 |

0.33 eV molecule$^{-1}$ less stable than the bridge site. The highest adsorption energies for the $NH_x$ fragments are obtained for NH in the hollow sites. We notice a substantial increase of the adsorption energy when the number of hydrogen atoms of the fragment is smaller. The favored binding site of the atomic nitrogen is hcp with an energy of −5.07 eV molecule$^{-1}$. Our results agree with the calculated values of Mavrikakis *et al.*[38] Atomic hydrogen binds much weaker than nitrogen, with an adsorption energy of −2.84 eV molecule$^{-1}$ for the most energetically favorable configuration, the fcc site, in agreement with the previous experimental study[39] and theoretical study.[38,40] Even with zero point energy correction the H atom shows a preference for the hollow sites. The potential energy surface of H on Rh(111) is more corrugated than adsorbed on other metals, e.g., Pt(111).[11] This is a key factor when determining the reaction paths which involve hydrogen.

We calculated the coadsorption energies for the combinations $NH_2$+H, NH+H, and N+H. This is important for the selection of the final states of the dehydrogenation reactions. For $NH_2$+H we calculated structures with different arrangements of the fragments in a $p(2\times2)$ unit cell. All NH+H systems are very stable on the Rh(111) surface, with coadsorption energies around −7 eV molecule$^{-1}$. As can be seen from Table II, for each group of coadsorbates the differences in coadsorption energies are small. Also the N+H systems are stable, with energies around −7.6 eV molecule$^{-1}$. In the last column we list the sum of the separated adsorption energies. The differences between the two columns actually represent the lateral interactions. In all the cases the lateral interactions are repulsive. Most are only a few tenths of an eV. At 0.25 ML coverage the lateral interactions play an important role in determining the activation barriers.

### B. Frequency analysis of $NH_x$ adsorbates on the Rh(111) surface

The frequencies for the vibration modes of the $NH_x$ adsorbed in the most stable adsorption sites on Rh(111) surface are summarized in Table III. All the stretching and deformation frequencies of adsorbed eclipsed ammonia have lower values than gaseous ammonia (calculated values: 3574,

TABLE III. Calculated harmonic frequencies (cm$^{-1}$) of the normal modes for $NH_x$ species adsorbed on $p(2\times2)$-Rh(111) surface. Experimental data are given in parenthesis (Ref. 5).

| Vibration mode | $NH_3$ top | $NH_2$ bridge | NH fcc | NH hcp |
|---|---|---|---|---|
| Asymmetric stretching, $\nu_{as}$ | 3521, 3520 (3197) | 3506 (3354) | 3453 | 3437 |
| Symmetric stretching, $\nu_s$ | 3367 (3065) | 3395 (3283) | | |
| Asymmetric scissoring, $\delta_{as}$ | 1555, 1554 (1634) | | | |
| Symmetric scissoring, $\delta_s$ | 1013 | 1462 | | |
| Wagging libration, $L_w$ | | 675 | | |
| Twisting libration, $L_t$ | | 636 | 686, 686 | 685, 685 |
| Tumbling (rocking) libration, $L_r$ | 555, 552 | 607 | | |
| Frustrated translation ⊥ to the surface, $T_\perp$ | 365 | 485 | 576 | 562 |
| Frustrated translation ∥ to the surface, $T_\parallel$ | 103, 96 | 328, 171 | 459, 459 | 427, 426 |
| Frustrated rotation, $R$ | 53 | | | |

TABLE IV. Calculated harmonic frequencies ($cm^{-1}$) of the normal modes for N and H species adsorbed on $p(2\times2)$-Rh(111) surface. Experimental data are given in parenthesis (Ref. 39).

| Vibration mode | N fcc | N hcp | H fcc | H hcp | H bridge | H top |
|---|---|---|---|---|---|---|
| $T_\perp$ | 541 | 560 | 1091 (1089) | 1091 | 1265 | 1966 |
| $T_\parallel$ | 467, 467 | 464, 447 | 786, 783 (637–726) | 746, 741 | 1032, *i*330 | 152, 149, 143, 107, 62, 59 |

3572, 3413, 1612, 1612, and 955 $cm^{-1}$), except the umbrella mode ($\delta_s$). The computed values for the vibrational frequencies in gas phase are practically the same as those calculated by Preuss *et al.*[24] and are in good agreement with the experimental values[41] (3450, 3413, 3337, 1628, 1628, and 968 $cm^{-1}$), the maximum error being less than 4%. For $NH_2$ in bridge position the stretching ($\nu_{as}$) frequency is lower than for $NH_3$ or for the calculated values for $NH_2$ in gas-phase (3410, 3303, and 1484 $cm^{-1}$). The librations (wagging, twisting, and rocking) and translations ($T_\perp$) and $T_\parallel$ modes have higher values than for $NH_3$. NH adsorbed in fcc and hcp sites give very similar values for the vibrations. The highest vibration is the stretching mode, but it is lower than for $NH_3$ and $NH_2$ and than the calculated value for NH in gas phase (3223 $cm^{-1}$). The twisting and the translation modes on the contrary, have higher energies than for $NH_3$ and $NH_2$. We notice that as the number of hydrogen atoms is lower in the $NH_x$ fragment the species have a higher stability on the surface and this leads to a decrease of the NH stretch vibrations and an increase in low frequencies modes. This tendency can be directly correlated also with the stability of $NH_x$ species on the Rh(111) surface.

The frequency of vibrations of $NH_x$ species adsorbed on Rh nanoparticles (4 nm) were recently experimentally studied by Leewis *et al.*[5] using attenuated total reflection Fourier transform infrared spectroscopy (ATR-FTIR). For substrate temperatures between 20 and 100 °C they observed N-H bend vibrations at 1606–1813 $cm^{-1}$ and stretch vibrations at 3065–3400 $cm^{-1}$. Our calculated frequencies are larger than these experimental values. They mentioned also large values for N-H stretch when $NH_3$ is adsorbed on Rh and silica or for bigger Rh nanoparticles (20 nm). The differences are small and they can be attributed to the hydrogen bonds between the adsorbed fragments and to the anharmonic contributions, which are not included in the calculations. The calculated frequencies of N adsorbed in hollow sites are even smaller than the frequencies given by the NH species, in agreement with their stability on the surface. The hydrogen atom shows the same behavior for all the adsorption sites.

The Rh-H stretching frequency is in very good agreement with the values experimentally determined by Mate *et al.*[42] and by Yanagita *et al.*[39] They gave different explanations for the origin of the H spectra on the Rh(111) surface. For the vibrations parallel with the surface both groups found a very broad band. The origin of this band was not clear. Yanagita *et al.* found in the EELS spectrum at 90 K a band around 637–726 $cm^{-1}$ and the highest frequency at 1089 $cm^{-1}$. These values agree very well with our calculated values. They explained the H spectra using the localized, classical harmonic-oscillator model. Mate *et al.* using HREELS at 80 K observed a very broad band around 450 $cm^{-1}$ which gives after deconvolution peaks of 350, 320, 210, and 470 $cm^{-1}$. Higher excitations were found at 750, 1100, and 1450 $cm^{-1}$. They explained the broadened energy-loss peaks as a result of the quantum delocalized nature of hydrogen adsorption. Above 0.4 ML the bandwidth is reduced due to the reduction of H mobility (blocking sites) and possible H-H interactions.

The vibrational analysis of the hydrogen atom indicates that the top and the hollow adsorption sites are minima on the potential energy surface, and the bridge is a transition state (see Table IV). In the case of H in fcc or hcp and on bridge sites the frequency values are similar; the differences are of the order of a few $cm^{-1}$. For the hollow sites we obtain the highest frequency for the Rh-H stretching vibration perpendicular on the metallic surface ($\nu_\perp$) at 1091 $cm^{-1}$, in excellent agreement with the experimental data. The hcp hollow site is the most stable adsorption site and the fcc site is slightly higher in energy (Table I). The minima are well-defined on the potential energy surface. The bridge site is clearly a transition state. We obtained three vibrational modes which include H contribution, one for the perpendicular vibration at 1265 $cm^{-1}$, one parallel to Rh-Rh bridge, and one with an imaginary frequency ($i330$ $cm^{-1}$), which is perpendicular to the Rh-Rh bridge. In the case of the H on top there is a strong coupling with the surface phonons and the H atom contributes to more vibration modes. H on top has a lower adsorption energy than adsorbed in bridge or hollow sites and consequently the Rh-H stretching frequency ($\nu_\perp$) has the highest value. The frequency analysis shows that H on top presents a shallow minimum and the vibration modes have a strong anharmonic contribution.

We have calculated also the frequencies for coadsorbed $NH_x$+H systems, in order to obtain the partition functions for the final states of $NH_x$ dehydrogenation reactions. The vibration modes are practically the same as for the simple adsorbates species. In the case of the transition states frequency analysis, we noticed that one of the high normal modes is lost and all the other frequencies have similar values, only slightly higher than for the correspondent $NH_x$ fragment. The frequency analysis of the $NH_x$, $NH_{x-1}$, and their associate transition states makes it possible to describe the minimum reaction paths (MEP) on the metallic surface.

### C. Reaction pathways for $NH_x$ dehydrogenation

The hydrogenation reactions of $NH_x$ fragments on the Rh(111) surface was previously studied by Liu *et al.*[7] using DFT. For each step they determined two transition states (TS1, TS2), using the breaking bond distance N–H as the reaction coordinate. For the N and NH hydrogenation the transition states are localized in a hcp hollow site, with the H

atom on the off-top (TS1) and almost in a fcc hollow site (TS2). In both situations there is a bonding competition effect, the fragments involved in hydrogenation reactions share bonding with the Rh surface atoms. As a consequence the height of the barriers is considerable, 0.99–1.29 eV. The hydrogenation of $NH_2$ has even a higher barrier, 1.24 eV (TS1) and 1.32 eV (TS2). In the following paper from the same group[13] Crawford *et al.* analyzed the factors which govern the minimum energy reaction pathways for NH and $NH_2$ hydrogenations on close-packed surfaces of the 4*d* transition-metals from Zr-Pd. They found that the potential energy surface of the H adsorbed on a metallic surface determines the activation barrier and the minimum reaction path, over the top or over the bridge.

Our results are comparable although there are some differences with respect to the activation barriers and to the minimum reaction paths. We studied the reversed reactions ($NH_x$ dehydrogenation) using the NEB method, an extensively and accurate method to determine the transition states. Frequency analysis was used to characterize on the potential energy surface the minima for reactants and products, and the maxima for the transition states. We considered different possibilities for the reaction paths for each dehydrogenation step and we described the role of the potential energy surface of the H.

#### *1. $NH_3$ dehydrogenation*

Starting from eclipsed ammonia on top the NEB method gives the following results (see Fig. 1). The minimum energy path leads in the first step to dissociation into $NH_2$ adsorbed in bridge position and the H atom in a hcp hollow site. At the transition state N–H bond is 1.79 Å (initially is 1.02 Å) and H–Rh is 1.66 Å. Although the N–H bond is substantially elongated in the transition state structure the N atom and the H atoms that form $NH_2$ have moved very little, meaning that there is neither an early nor a late transition state. After the N–H bond breaks, H falls in the neighboring hollow site. The $NH_2$ fragment goes towards the bridge, not too far from the initial position. In the final state $NH_2$ and H are coadsorbed and they share a Rh atom. This first dehydrogenation step has the highest barrier, 1.36 eV. If the zero point energy correction is included, the barrier becomes 1.1 eV. Another possibility is with the H ending in a fcc hollow site; but the activation barrier and the structure of the transition state are very similar. Each dehydrogenation step can be followed by diffusion of the fragments, lowering the energy by 0.1 to 0.2 eV.

#### *2. $NH_2$ dehydrogenation*

In the next step another atom is removed from the $NH_2$ fragment, which is initially adsorbed in a bridge position. In the final state NH and H can be adsorbed in any of the hollow sites. The difference in coadsorption energy between different combinations is almost 0.12 eV (see Table II). We calculated the reaction paths for two cases, with NH fcc+H fcc and NH hcp+H hcp as final states. In both situations the H atom tilts to the neighboring hollow site and successively goes over a bridge position to its final position. At transition states the NH fragment is almost in its final hollow site position. The structures of the transition states are similar, but with the fragments interchanged. The N–H bonds are equally stretched. The H atom is still connected to the N atom and one metal atom, common with the NH fragment. The activation barriers are high, 1.07 and 1.18 eV or 0.84 and 0.95, respectively, if the ZPE corrections are taken into account. Notice that the second transition state has a higher barrier, suggesting the assymetry of the PES for the bridge positions.

#### *3. NH dehydrogenation*

The last step is the NH dissociation. Again all combinations for N and H in the fcc and/or hcp hollow sites in the final state are possible (see Table II). NH and N are strongly adsorbed in hollow sites and in all these situations the N atom will remain in the initial position. We calculated the energy paths for three situations. For N hcp+H hcp and N hcp+H fcc as final states the transitions states are very similar. In both cases the H atom will move over the top in a neighbor hollow site. The energy barriers are 1.15 or 0.99 eV if the ZPE correction is considered.

We calculated the reaction path also in the case of NH fcc$\rightarrow$N fcc+H fcc. Here the barrier for N-H bond breaking is higher (1.39 eV). The bond breaking and the H diffusion take place sequentially, not as in the previous case just mentioned. The activation barrier is determined by the bond breaking, while the H diffusion has no barrier. We obtained two imaginary frequencies for the stationary point of this reaction path. One frequency is similar with the imaginary frequencies of the previous NH dehydrogenations ($i1204$ cm$^{-1}$). The other ($i206$ cm$^{-1}$) represents the rotation in the plane of the NH fragment perpendicular on the bridge position (see Fig. 1). The H atom is not in the top position as in the previous case, but in the bridge-hollow position. The potential energy surface has a maximum along the line connecting two top sites. The existence of the imaginary NH rotation mode means that the system wants to shift the H atom to the top, where one will find the minimum path as in the transition states described above. We conclude that this point is not a transition state as is described in the harmonic transition state theory. The existence of the secondary stationary point for NH over the bridge agrees with the conclusion of Crawford *et al.*[13] that the H atom determines the minimum reaction path for NH dissociation.

Other possibilities for $NH_x$ dissociation were also taken into account and due to the symmetry of the surface we obtained similar results. We searched with NEB possible transition states but the frequency analysis validated the results only for the cases discussed above.

#### *4. Classification of the transition states*

The transition states have intermediate structures between reactants and products. They are situated closer on the PES to one of them and the structure will be as well more similar than with the other minima. We can classify the transition states as early or late, depending on the resemblance with the reactants (here $NH_x$) and the final products ($NH_{x-1}$). In the reactions discussed above there are actually two processes

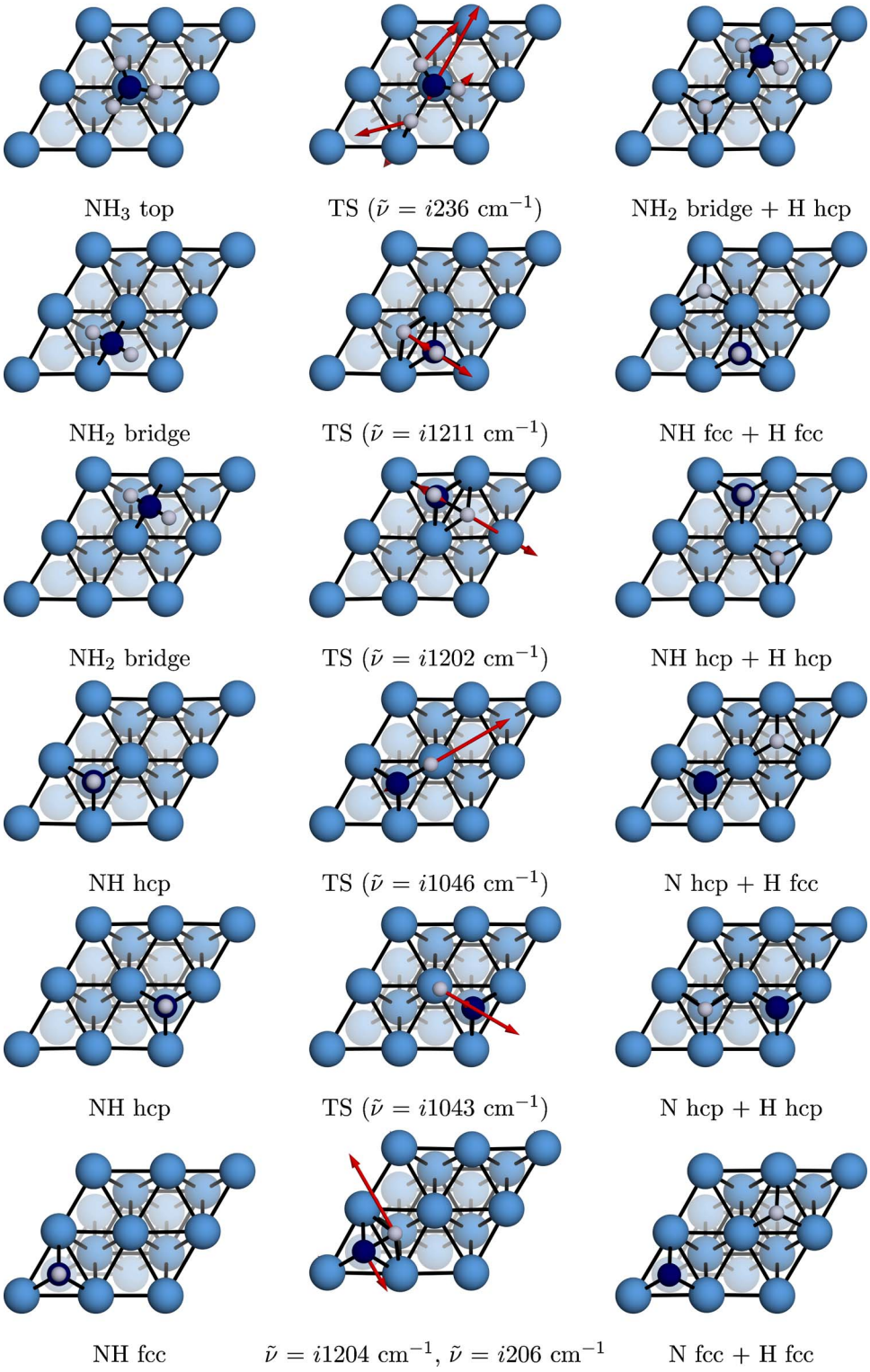


FIG. 1. (Color online) Ammonia decomposition on $p(2\times2)$-Rh(111) surface (top view). For the transition states the eigenvectors of the imaginary frequencies are given.

which occur, the N–H bond breaking and the diffusion of the H atom. The reaction profiles along the minimum energy paths (MEP) reveal that for the dehydrogenation reactions the activation barriers are given by the N-H bond breaking. The H diffusion has practically no barrier.

To describe this resemblance of structures and how early or late the transition states are, we discuss here the variation of the N–H distance for the bond that will break during a reaction. Table V gives for comparison the length of the N-H bond that will break in the initial reaction and the transition states for the $NH_x$ dehydrogenation reactions. For the transition state of the $NH_3$ dehydrogenation, the N–H distance in the transition state is 75% elongated with respect to the initial distance. The bond is practically broken and we can say that in this respect the reaction is rather late. For the other transition state the N–H distance increases by around 33% with respect to the initial values. This explains also the high barrier of the $NH_x$ dehydrogenation.

TABLE V. N–H distances (Å) for reactants $d_{\text{N-H}}(\text{R})$ (the second column) and transition states $d_{\text{N-H}}(\text{TS})$ (the third column). The next columns estimate if the transition state is late (high percentages) or early (low percentages). The fourth column presents the percentage of the covered energy path at the transition state with respect to the H atom which splits off. The fifth column expresses the covered energy path at the transition state but with respect to the whole system. $d_{\text{R-TS}}$ is the distance in the configuration space between reactant and transition state. $d_{\text{TS-P}}$ is the distance in the configuration space between transition state state and product state.

| Reaction | $d_{\text{N-H}}(\text{R})$ | $d_{\text{N-H}}(\text{TS})$ | $\frac{d_{\text{R-TS}}}{d_{\text{R-TS}}+d_{\text{TS-P}}}100\%$ (for H) | $\frac{d_{\text{R-TS}}}{d_{\text{R-TS}}+d_{\text{TS-P}}}100\%$ |
|---|---|---|---|---|
| $NH_3$ top$\rightarrow NH_2$ bridge+H hcp | 1.02 | 1.79 | 62.5 | 39 |
| $NH_2$ bridge$\rightarrow$NH fcc+H fcc | 1.02 | 1.37 | 40.5 | 46 |
| $NH_2$ bridge$\rightarrow$NH hcp+H hcp | 1.02 | 1.36 | 39.4 | 45 |
| NH hcp$\rightarrow$N hcp+H hcp | 1.04 | 1.53 | 44.1 | 44 |
| NH hcp$\rightarrow$N hcp+H fcc | 1.04 | 1.52 | 30.5 | 44 |

Another approach to discuss how early or late a transition state occurs is to consider the distance in the configuration space between the states involved in a reaction (reactant, transition state, product). Table V gives the ratios of the distances in the configuration space between reactant and transition state ($d_{\text{R–TS}}$) and the sum of the distances between reactant and transition state ($d_{\text{R–TS}}$) and transition state and product ($d_{\text{TS–P}}$), $\frac{d_{\text{R–TS}}}{d_{\text{R–TS}}+d_{\text{TS–P}}}100\%$. We calculate the distances using only the coordinates of the H which splits off and using all coordinates of the system. These values are estimates of where the transition state is along the reaction path. The ratios are relative to the length of the reaction path, depending on how far the H atom will diffuse to the final state. If we consider the ratios with respect only to the H atom which splits off (the fourth column), this atom being the species with the highest mobility on the surface during a reaction, the first reaction ($NH_3$ dehydrogenation) occurs latish, and all the other reactions are early to half-way. The conclusion is the same as when we previously considered the variation of the N–H distances. The other atoms, especially the metallic ones, do not change their position too much during reactions and their displacements express a global effect. The last column from Table V presents the same ratios but with respect to the distances in the configuration space for all the atomic coordinates in the system. With respect to the entire system, all the reactions can be considered to occur early to half-way.

### D. Kinetics and thermodynamics

The kinetic and thermodynamic parameters for the reactions discussed above are summarized in Table VI. The stability of the $NH_x$ fragments on the Rh surface increase when $x$ decreases. But going from $NH_x$ to $NH_{x-1}$+H the difference in energy is rather small (see Fig. 2). As a consequence the dehydrogenation reactions are slightly endothermic, with overall reaction energies between 0.05 and 0.35 eV, prior to diffusion of hydrogen away from the N containing species. Including the H diffusion all the reactions become exothermic. The barrier heights are large. The ammonia dissociation has the highest barrier (1.36 eV) but also the subsequent reactions have high barriers, over 1 eV.

The ZPE corrections, as we expected, have important values (0.6–1 eV) for $NH_3$, $NH_2$+H, and $NH_2$ fragments and their transition states. The most significant ZPE corrections we obtained were in the cases of an ammonia molecule

TABLE VI. Thermodynamic and kinetic parameters for $NH_x$ dehydrogenation/hydrogenation on $p(2\times2)$-Rh(111) surface calculated at a temperature of 300 K. $\Delta E$ is the heat of reaction ($E_{\text{P}}-E_{\text{R}}$), $E_{bar}$ is the barrier height without zero point contribution ($E_{\text{TS}}-E_{\text{R}}$), ZPE is the zero point energy contribution, $E_{act,0}$ is the activation energy from Eq. (7), $E_{act}$ is the activation energy from fitting the rate constants to an Arrhenius form [Eq. (2)], $\Delta S_0^{\#}$ is the activation entropy, and $\nu^*$ is the preexponential factor.

| | Reaction | $\Delta E$ (eV) | $E_{bar}$ (eV) | ZPE (eV) | $E_{act,0}$ (eV) | $E_{act}$ (eV) | $\Delta S_0^{\#}$ (J mol$^{-1}$ K$^{-1}$) | $\nu^*$ ($10^{+13}$ s$^{-1}$) |
|---|---|---|---|---|---|---|---|---|
| 1. | $NH_3$ top$\rightarrow NH_2$ bridge+H hcp | 0.18 | 1.36 | 0.26 | 1.10 | 1.13 | 2.1 | 2.18 |
| 2. | $NH_2$ bridge+H hcp$\rightarrow NH_3$ top | −0.18 | 1.18 | 0.12 | 1.06 | 1.10 | 40.6 | $1.90\times10^2$ |
| 3. | $NH_2$ bridge$\rightarrow$NH fcc+H fcc | 0.05 | 1.07 | 0.23 | 0.84 | 0.86 | −0.1 | 1.68 |
| 4. | NH fcc+H fcc$\rightarrow NH_2$ bridge | −0.05 | 1.02 | 0.08 | 0.94 | 0.97 | 9.3 | 5.03 |
| 5. | $NH_2$ bridge$\rightarrow$NH hcp+H hcp | 0.07 | 1.18 | 0.23 | 0.95 | 0.97 | −1.3 | 1.46 |
| 6. | NH hcp+H hcp$\rightarrow NH_2$ bridge | −0.07 | 1.11 | 0.08 | 1.02 | 1.05 | 7.4 | 4.03 |
| 7. | NH hcp$\rightarrow$N hcp+H hcp | 0.38 | 1.15 | 0.16 | 0.99 | 1.01 | 1.9 | 2.11 |
| 8. | N hcp+H hcp$\rightarrow$NH hcp | −0.38 | 0.77 | 0.04 | 0.73 | 0.75 | 3.7 | 2.60 |
| 9. | NH hcp$\rightarrow$N hcp+H fcc | 0.35 | 1.15 | 0.16 | 0.99 | 1.01 | 1.9 | 2.11 |
| 10. | N hcp+H fcc$\rightarrow$NH hcp | −0.35 | 0.80 | 0.03 | 0.77 | 0.79 | 2.9 | 2.39 |

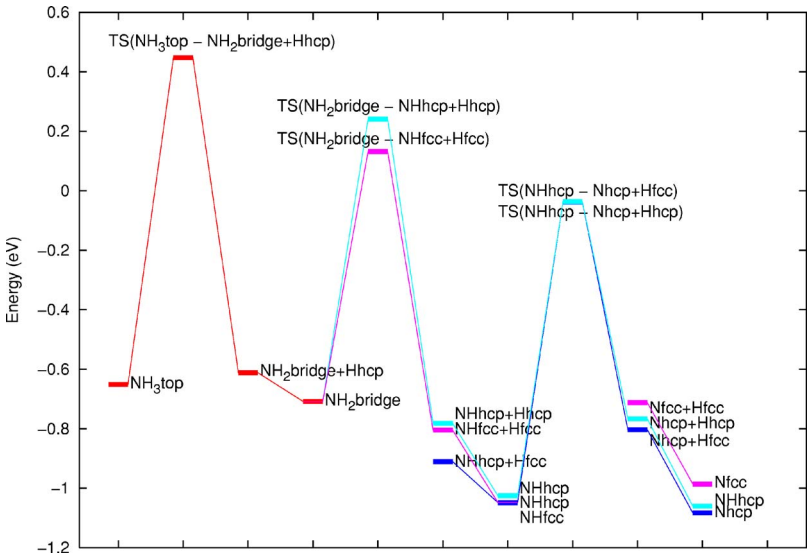


FIG. 2. (Color online) Potential energy profile for the $NH_3$ dehydrogenation over the Rh(111) surface. The energies include ZPE correction. The reference is given with respect to $NH_3$ in gas phase and Rh slab. Each step can be followed by the H atom diffusion far on the surface.

(1.01 eV) and for $NH_2$ (0.7 eV). They do not change the order of the activation barriers, except in the case of $NH_2$ bridge dehydrogenations, when the reverse reactions require higher activation barriers. With the ZPE correction the barriers heights remain still high, with values between 0.87 and 1.13 eV. The rate limiting step of ammonia dehydrogenation is the first reaction, $NH_3$ top$\rightarrow NH_2$ bridge+H hcp. $NH_2$ bridge$\rightarrow$NH fcc+H fcc has the highest reaction rate and all the other elementary reactions have intermediate reaction rates.

The $NH_3$ desorption energy (0.65 eV) is much lower than the dehydrogenation barrier (1.13 eV). That means from a thermodynamic point of view that the ammonia rather desorbs than dissociates. But the competition between desorption and dissociation phenomena can be controlled in practice via the applied pressure and temperature (200 Torr and higher, over 1000 K), which will shift the equilibrium towards the reactants or towards the products.[3,8,43,44] Another important aspect is that the equilibrium between these competitive processes can be influenced by steps. Calculations on steps would be a natural follow-up of our calculations in this paper.

As we showed in the frequency analysis, the contribution to the partition functions of low frequency modes is important for entropic contributions. Consequently, $NH_3$ has a high entropy because of the almost free rotation around its axis. This mode is still present in the transition state of the first dehydrogenation. It has also a low excitation energy and consequently this transition state has a high entropy too. For all other reactants, products, intermediates, and transition states the entropy is small because the vibrations have relatively high frequencies.

For the reactions this means that the activation entropies are small, except for the hydrogenation of $NH_2$. The reason is that the transition state of this reaction is loose (i.e., it has a high entropy). The reverse reaction, $NH_3$ dehydrogenation, does not have a high activation entropy because also $NH_3$ has a high entropy.

The activation entropy is related to the reaction prefactors as shown in Ea. (8). All, except one reaction, have prefactors of the order of $10^{+13}$ $s^{-1}$, which corresponds to a low activation entropy. Only the hydrogenation of $NH_2$ has a high prefactor, $19\times10^{+15}$ $s^{-1}$.

Also the values for the activation energies obtained from Arrhenius equation (2) are listed in Table VI. We calculated the activation energies from a linear regression of $\ln(k)$ as a function on $1/T$ plots for temperatures between 100 and 1000 K. In this range all the reaction rates follow the linear dependence from the Arrhenius equation. The obtained values for activation energies are very close to the values of the ZPE corrected activation energies of Eq. (7). The difference is about 0.02 to 0.03 eV.

## IV. CONCLUSIONS

We have presented DFT results for the elementary steps of the ammonia dissociation and reversed reactions on the Rh(111) surface. The calculations lead to a consistent image of the stability of $NH_x$ fragments. The most stable species on the surface are NH and N, with adsorption energies of −4.17 and −4.98 eV, respectively. We have described the normal vibrational modes for $NH_x$ species, which are in agreement with available experimental data. The ammonia molecule behaves as a free rotator on the Rh(111) surface. The frequency analysis showed that the H atom presents a rather corrugated potential energy surface, providing insight into the minimum reaction paths.

The nudged elastic band method was used to determine the transition states for the elementary reactions. Due to similar coadsorption energies for some $NH_x$+H systems for each dehydrogenation step we have studied different minimum reaction paths. With respect to the overall change of the initial state structures the transition states can be regarded neither early nor late. Around 39% to 46% from the minimum reaction paths already occurred at the transition states. If only the displacement of the H atom which is removed is considered, the $NH_3$ dehydrogenation can be considered late.

Using the vibrational analysis we were able to determine the partition functions and the related thermodynamic and kinetic properties of ammonia decomposition and reverse re-

actions. The dehydrogenation reactions are endothermic, with reaction energies between 0.05 and 0.35 eV. The calculated activation barriers are quite high. The zero point energy corrections give significant contributions, especially in the case of ammonia dehydrogenation (0.26 eV). Taking into account the zero point energy corrections, the barriers lower to values between 0.73 and 1.1 eV. The first reaction, $NH_3$ dehydrogenation, is the rate limiting step with an activation energy of 1.1 eV. The activation entropies are small and the preexponential factors are determined by the $ek_BT/h$ factor ($10^{+13}$ $s^{-1}$). The only exception is the $NH_3$ dehydrogenation, where we calculated a large entropic effect. The preexponential factor raises to $10^{+15}$ $s^{-1}$. The large zero point energy correction, the highest barrier energy, the significant entropic effect, and preexponential factor present the $NH_3$ dehydrogenation as the most interesting step in ammonia dehydrogenation/hydrogenation.

## ACKNOWLEDGMENTS

This research was financially supported by the Foundation for Fundamental Research on Matter (FOM), The Netherlands, and the Dutch National Computing Facilities Foundation, SARA. C.P. thanks Joost de Greef for the visualization program and Peter Vassilev for the fruitful and nice discussions.

*Email address: c.popa@tue.nl

[1] G. Busca, L. Lietti, G. Ramis, and F. Berti, Appl. Catal., B **18**, 1 (1998).
[2] R. M. van Hardeveld, R. A. van Santen, and J. W. Niemantsverdriet, J. Vac. Sci. Technol. A **15**, 1558 (1997).
[3] S. Stolbov and T. S. Rahman, J. Chem. Phys. **123**, 204716 (2005).
[4] J. C. Ganley, F. S. Thomas, E. G. Seebauer, and R. I. Masel, Catal. Lett. **96**, 117 (2004).
[5] C. M. Leewis, W. M. M. Kessels, M. C. M. van de Sanden, and J. W. Niemantsverdriet, Appl. Surf. Sci., doi:10.1016/j.apsusc.2005.12.115 (2006).
[6] F. Frechard, R. A. van Santen, A. Siokou, J. W. Niemantsverdriet, and J. Hafner, J. Chem. Phys. **111**, 8124 (1999).
[7] Z.-P. Liu, P. Hu, and M.-H. Lee, J. Chem. Phys. **119**, 6282 (2003).
[8] A. Logadóttir and J. K. Nørskov, J. Catal. **220**, 273 (2003).
[9] C. J. Zhang, M. Lynch, and P. Hu, Surf. Sci. **496**, 221 (2002).
[10] G. Novell-Leruth, A. Valcarcel, A. Clotet, J. Ricart, and J. Perez-Ramirez, J. Phys. Chem. B **109**, 18061 (2005).
[11] W. K. Offermans, A. P. J. Jansen, and R. A. van Santen, Surf. Sci. **600**, 1714 (2006).
[12] A. Bilić, J. R. Reimers, N. S. Hush, and J. Hafner, J. Chem. Phys. **116**, 8981 (2002).
[13] P. Crawford and P. Hu, J. Chem. Phys. **124**, 044705 (2006).
[14] G. Kresse and J. Furthmüller, Comput. Mater. Sci. **6**, 15 (1996a).
[15] G. Kresse and J. Furthmüller, Phys. Rev. B **54**, 11169 (1996b).
[16] D. Vanderbilt, Phys. Rev. B **41**, 7892 (1990).
[17] G. Kresse and J. Hafner, J. Phys.: Condens. Matter **6**, 8245 (1994).
[18] J. P. Perdew, in *Electronic Structure of Solids'91*, edited by P. Ziesche and H. Eschrig (Akademie Verlag, Berlin, 1991), pp. 11–20.
[19] A. Bogicevic and K. C. Hass, Surf. Sci. **506**, L237 (2002).
[20] B. Hammer, Surf. Sci. **459**, 323 (2000).
[21] B. Hammer, Faraday Discuss. **110**, 323 (1998).
[22] C. Kittel, in *Introduction to Solid State Physics*, 8th ed., edited by S. Johnson and P. McFaden (Wiley, New York, 2005).
[23] O. Dubay and G. Kresse, Phys. Rev. B **67**, 035401 (2003).
[24] M. Preuss and F. Bechstedt, Phys. Rev. B **73**, 155413 (2006).
[25] J. Hafner, J. Mol. Struct. **661-653**, 3 (2003).
[26] G. K. A. Eichler and J. Hafner, J. Phys.: Condens. Matter **8**, 7659 (1996).
[27] G. Sun, J. Kurti, P. Rajczy, M. Kertesz, J. Hafner, and G. Kresse, J. Mol. Struct.: THEOCHEM **624**, 37 (2003).
[28] C. Bae, D. E. Freeman, J. D. Doll, G. Kresse, and J. Hafner, J. Chem. Phys. **113**, 6926 (2000).
[29] P. J. Feibelman, Phys. Rev. B **67**, 035420 (2003).
[30] G. Mills, H. Jónsson, and G. K. Schenter, Surf. Sci. **324**, 305 (1995).
[31] G. Henkelman, G. Jóhannesson, and H. Jónsson, in *Theoretical Methods in Condensed Phase Chemistry*, edited by S. D. Schwartz, Vol. 5 of Progress in Theoretical Chemistry and Physics (Kluwer, Dordrecht, 2000), Chap. 10, pp. 269–300.
[32] G. Henkelman, B. P. Uberuaga, and H. Jónsson, J. Chem. Phys. **113**, 9901 (2000b).
[33] G. Henkelman and H. Jónsson, J. Chem. Phys. **113**, 9978 (2000).
[34] P. Maragakis, S. A. Andreev, Y. Brumer, D. R. Reichman, and E. Kaxiras, J. Chem. Phys. **117**, 4651 (2002).
[35] R. A. van Santen and J. W. Niemantsverdriet, *Chemical Kinetics and Catalysis* (Plenum Press, New York, 1995).
[36] I. Chorkendorff and J. W. Niemantsverdriet, *Reaction Rate Theory* (Wiley-VCH, Weinheim, 2003), Chap. 3, pp. 79–128.
[37] M. Garcia-Hernández, N. López, I. de P. R. Moreira, J. C. Paniagua, and F. Illas, Surf. Sci. **430**, 18 (1999).
[38] M. Mavrikakis, J. Rempel, J. Greeley, L. B. Hansen, and J. K. Nørskov, J. Chem. Phys. **117**, 6737 (2002).
[39] H. Yanagita, H. Fujioka, T. Aruga, and M. Nishijima, Surf. Sci. **441**, 507 (1999).
[40] S. Wilke, V. Natoli, and M. H. Cohen, J. Chem. Phys. **112**, 9986 (2000).
[41] G. Herzberg, in *Molecular Spectra and Molecular Structure*, edited by V. N. Reinhold (Van Nostrand Reinhold, New York, 1945).
[42] C. M. Mate and G. A. Somorjai, Phys. Rev. B **34**, 7417 (1986).
[43] S. Dahl, A. Logadottir, C. J. H. Jacobsen, and J. K. Nørskov, Appl. Catal., A **222**, 19 (2001).
[44] H. Mortensen, L. Diekhöner, A. Baurichter, E. Jensen, and A. C. Luntz, J. Chem. Phys. **113**, 6882 (2000).